Well-Aligned Ternary $Cd_{1-x}Zn_xS$ Nanowire Arrays and Their Composition-Dependent Field Emission Properties

Yi-Feng Lin,[†] Yung-Jung Hsu,[†] Shih-Yuan Lu,*[,†] Kuan-Tsung Chen,[‡] and Tseung-Yuen Tseng[‡]

Department of Chemical Engineering, National Tsing-Hua University, Hsinchu, Taiwan 30043, Republic of China, and Department of Electronics Engineering, National Chiao-Tung University, Hsinchu, Taiwan 30050, Republic of China

Received: May 27, 2007; In Final Form: July 4, 2007

Well-aligned plain CdS and ternary $Cd_{1-x}Zn_xS$ nanowire arrays were successfully fabricated via a noncatalytic and template-free metal−organic chemical vapor deposition process. The nanowires were grown on a 1 μm thick buffer layer formed in situ on the surface of silicon substrates. These nanowires were 20−40 nm in diameter and 500−900 nm in length. High-resolution transmission electron microscopy analyses revealed that the nanowires were single-crystalline and grew along the [0001] direction of the hexagonal crystalline phase. The photoluminescence characterizations showed near band edge emissions at 535, 498, and 473 nm for the CdS nanowire arrays and $Cd_{1-x}Zn_xS$ nanowire arrays with x values of 0.21 and 0.44, respectively, demonstrating clear color tunability achieved with the composition adjustment of the alloy nanowires. The same morphology and single-crystallinity of these three nanowire arrays enabled investigation of the composition-dependent field emission characteristics of the nanowire arrays for the first time, excluding interferences originating from morphology and crystallinity related factors. The plain CdS nanowire arrays exhibited better field emission properties, a lower turn-on field, and a higher field enhancement factor than the ternary $Cd_{1-x}Zn_xS$ nanowire arrays, for which the lower resistivity of the CdS nanowires may have played an important role. An important parameter, the absolute field enhancement factor (β_0), to more intrinsically quantify the field emission performance of the plain CdS and ternary $Cd_{1-x}Zn_xS$ nanowires arrays was also studied. The values of β_0 decreased with increasing Zn content in the ternary products. The high β_0 values of the CdS based nanowire arrays, comparable to that of carbon nanotubes grown on silicon wafers, made these nanowire arrays a promising candidate material for high-performance field emitting devices.

Introduction

One-dimensional (1-D) multiple-component nanostructures, such as coaxial core−shell,[1] superlattice,[2] and alloyed[1a,3] nanowires, have drawn much research attention in recent years because of their unique optoelectronic properties and potential applications in nanoscale device fabrication.[4] Among them, materials with ternary alloyed nanostructures may offer more unique properties than the corresponding plain and binary compounds,[5] and by adjusting the stoichiometry of the constituent components, their properties can be effectively tuned.[6] For example, $Cd_{1-x}Zn_xS$ nanowires,[1a] $Cd_{1-x}Zn_xSe$ nanowires,[3c] and CdS_xSe_{1-x} nanobelts[3a] were shown to possess color tunable emissions by adjusting the compositional ratios of Cd to Zn and S to Se of the nanostructures, respectively. $Cd_{1-x}Zn_x$ S nanoribbons, fabricated with a vapor transport process, have been demonstrated their wavelength controlled lasing properties.[3b] It has also been shown that the adjustment of composition in $Cd_{1-x}Zn_xS$ films led to optimization for the photoelectrochemical properties of the films.[7]

For practical applications in many fields, well-aligned 1-D nanostructures such as nanowire[8a] and nanotube[8b] arrays are often desirable to acquire full utilization of the benefit associated with the 1-D structure and to enable direct integration of the nanostructure to the targeted devices. For example, for field emission applications, good alignment of the 1-D nanostructure and good contact between the nanostructure and the substrate are essential to the success of the device. In applications involving mass transfer of participating chemical species and functioning charge carriers, for example, sensors and solar cell and fuel cell electrodes, alignment of the 1-D nanostructure provides straight transfer paths for the diffusing reactant and product molecules and direct shortcuts for the transport of charge carriers. Consequently, well-aligned arrays of 1-D nanostructures of relevant functional materials are of the first priority in the relevant synthetic and experimental designs. Wang and Song successfully prepared aligned ZnO nanowire arrays on *c*-plane sapphire substrates via a vapor−liquid−solid (VLS) process and demonstrated their functionality as a piezoelectric nanogenerator to convert mechanical energy into electric energy.[9a] Law et al.[9b] also synthesized ZnO nanowire arrays but on a ZnO-seeded F/SnO_2 conductive glass with an aqueous solution process. The ZnO nanowire arrays were used as the anode of a dye-sensitized solar cell (DSSC) to convert optical energy to electric energy.[9b] In addition, our previous work showed that well-aligned CdS nanowire arrays can be fabricated through a noncatalytic and template-free MOCVD process.[10] The as-grown CdS nanowire arrays exhibited excellent field emission properties, with which CdS nanowire arrays may be considered a promising candidate material for high-current field emitters and high-brightness electron sources.

* Corresponding author. E-mail: sylu@mx.nthu.edu.tw; tel.: +886-3-571-4364; fax: +886-3-571-5408.
[†] National Tsing-Hua University.
[‡] National Chiao-Tung University.

10.1021/jp074094b CCC: $37.00
Published on Web 08/21/2007

There have been many synthetic routes developed for the fabrication of 1-D nanostructure arrays. These many processes may be roughly divided into two general categories: liquid- and gas-phase processes. For the liquid-phase processes, such as template assisted electrochemical deposition, it is not easy to obtain good quality single-crystalline products, which are critical for applications demanding fast charge carrier transport within the 1-D nanostructure, particularly for semiconducting materials. It is also troublesome to remove the template and/or to clean the products. On the other hand, the creation of 1-D nanostructure arrays in gas-phase processes often involves catalyst seeds for induction anisotropic growth of the desired materials. The catalyst seeds may interfere with the potential application of the products, the removal of which may damage or contaminate the nanostructure. In view of the previous statements, there have been research efforts devoted to develop noncatalytic, template-free gas-phase processes for the production of 1-D nanostructure arrays.[3c,8a,10,11] 1-D nanostructure arrays of single-component and core−shell morphologies have been successfully fabricated with such attempts. The present work takes the approach one step further to produce 1-D nanowire arrays of alloyed semiconductors, $Cd_{1-x}Zn_xS$. With the ability to adjust the composition of the alloy nanowire arrays, we can not only investigate the emission tunability but also study the effect of composition on the field emission properties of the products.

It is well-known that field emission properties of semiconductor materials depend on several key factors including shape, size, alignment, tip sharpness, composition, spatial distribution, crystallinity, aspect ratio, etc. Zhao et al.[12] prepared and compared the field emission performance of three ZnO arrays of different shapes. Among them, the ZnO nanoneedle arrays exhibited much better field emission performance than arrays of nanocavities and nanobottles.[12] This difference can be clearly attributed to the 1-D shape and sharp tips of the array component. Lee et al.[13] incorporated Mg into ZnO and studied its effect on the band gap, photoluminescence (PL), and field emission of the products.[13] The incorporation of Mg changed the shape, size, alignment, aspect ratio, and spatial distribution of the ZnO nanorods and thus the field emission performance of the arrays.[13] In this work, $Cd_{1-x}Zn_xS$ nanowire arrays with three different Zn compositions (x) were fabricated with a noncatalytic, template-free metal−organic chemical vapor deposition (MOCVD) process. The products possessed similar shape, size, alignment, tip sharpness, spatial distribution, crystallinity, and aspect ratio, and thus, composition is the only significant variable among the products. With these nanowire arrays available, one can examine the composition effect on the field emission of the alloyed nanowires without significant interferences coming from other important factors such as shape, size, alignment, etc. The PL emission tunability of these $Cd_{1-x}Zn_xS$ nanowire arrays was also demonstrated.

For field emission efficiency, data of the turn-on field and threshold field are often reported. The criteria for these two quantities, however, are not universally established, and sometimes it is difficult to make a comparison between different measurements. Furthermore, these two parameters are in fact dependent on the interelectrode spacing, d, used in the measurement. Some researchers report a field enhancement factor, β, if the field emission data follow the Fowler−Nordheim (F−N) law. Again, the field enhancement factor depends on the interelectrode spacing and is not an intrinsic indicator for field emission efficiency. Zhong et al. proposed a two-region field emission (TRFE) model and defined a more intrinsic indicator called the absolute enhancement factor, β_0, which is independent of d and V, to quantify the field emission efficiency of an emitter.[14] In this work, the absolute field enhancement factor of the $Cd_{1-x}Zn_xS$ nanowire arrays and its variation over the composition of the nanowire are reported for the first time. The absolute enhancement factor of the CdS nanowire array, 7813, was found to be comparable to that of carbon nanotubes grown on a silicon wafer, 7900.[14a] This further demonstrates the potential of CdS nanowire arrays as a promising alternative for field emission applications.

Experimental Procedures

Preparation of Plain CdS and Ternary $Cd_{1-x}Zn_xS$ Nanowire Arrays. Plain CdS and ternary $Cd_{1-x}Zn_xS$ nanowire arrays were fabricated with a hot-wall MOCVD process operated in a three-zone horizontal tube furnace by using silicon plates as the substrates. We have prepared randomly oriented $Cd_{1-x}Zn_xS$ nanowires with a gold nanoparticle assisted MOCVD process through the −−VLS growth mechanism.[1a] In this work, we take the synthetic development one step further by producing well-aligned $Cd_{1-x}Zn_xS$ nanowire arrays through proper control of processing conditions with no external catalysts or sacrificial templates used. Dialkyldithiocarbamate based single-source precursors of CdS ($Cd(S_2CN(C_3H_7)_2)_2$, denoted as Cd33, 0.1 g) and ZnS ($Zn(S_2CN(C_2H_5)_2)_2$, denoted as Zn22, 0.05 g) were utilized for production of the nanowire arrays.[15] The detailed synthetic procedures for Cd33 used in this work were documented in our previous work.[15a,b] Zn22 was purchased from Aldrich and used as received. For the production of plain CdS nanowire arrays, Cd33 was fed into a precursor boat and heated to 160 °C to generate precursor vapors. The furnace temperature was set at 450 °C, and the deposits were collected at regions of deposition temperature of around 300 °C. As for the fabrication of the ternary $Cd_{1-x}Zn_xS$ nanowire arrays, Cd33 and Zn22 were fed into two separate precursor boats and heated to different temperatures (Cd33 at 160 °C and Zn22 at 140 °C) to generate suitable amounts of mixed precursor vapors. The vapors of the co-fed precursors were further introduced into the furnace by the carrier gas, N_2. The furnace temperature was also set at 450 °C, and two deposits were collected at regions of deposition temperatures of 300 and 400 °C, respectively. All depositions were run for 6 h with a carrier gas flow rate of 50 sccm and a system pressure of 30 Torr. After the MOCVD process, the as-deposited ternary nanowires were further annealed at 500 °C for 48 h in a nitrogen atmosphere.

Characterizations. The morphology and dimension of the as-deposited nanowires were examined by field emission scanning electron microscopy (FESEM, Hitachi, S-4700). The crystallographic structures of the nanowires were investigated by X-ray diffraction (XRD, MAC Sience MXP18), transmission electron microscopy (TEM, JEOL JEM-2010, operated at 200 kV), and high-resolution TEM (HRTEM, JEOL JEM-400EX, operated at 400 kV). The elemental analyses of individual nanowires were conducted with an energy dispersive spectrometer (EDS), an accessory of the TEM (JEM-2010). For PL spectroscopy, a Hitachi F-4500 spectrometer equipped with a xenon lamp (150 W) and a 700 V photomultiplier tube as the detector was used. The excitation wavelength was set at 350 nm. The field emission measurements of the nanowire arrays were conducted in a vacuum chamber maintained at a pressure of 10^{-6} Torr. A copper electrode probe was taken as the anode with an area of 7.1×10^{-3} cm^2. The anode was placed at a distance of 200−400 μm from the tips of the nanowires during the measurement.

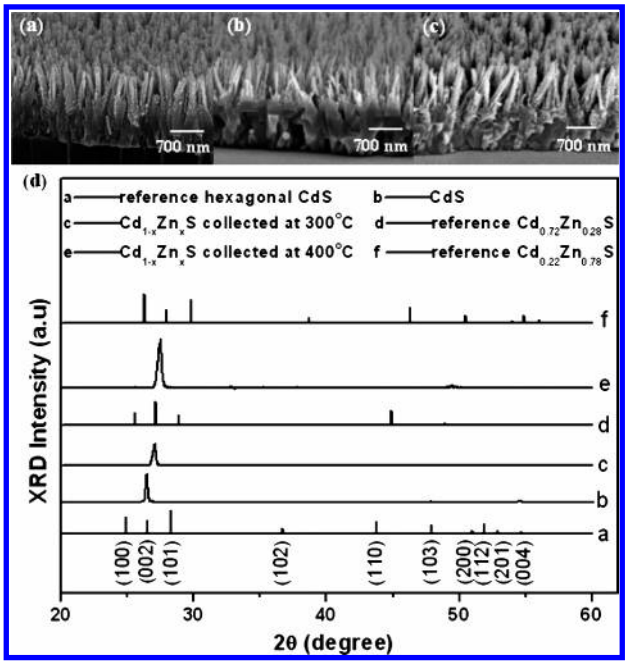

Figure 1. SEM images of (a) CdS deposits collected at 300 °C with a deposition time of 6 h, (b) $Cd_{1-x}Zn_xS$ deposits collected at 300 °C with a deposition time of 6 h and annealing time of 48 h, and (c) $Cd_{1-x}Zn_xS$ deposits collected at 400 °C with a deposition time of 6 h and annealing time of 48 h. (d) XRD patterns of CdS deposits and $Cd_{1-x}Zn_xS$ deposits annealed for 48 h.

Results and Discussion

Well-aligned plain CdS and ternary $Cd_{1-x}Zn_xS$ nanowire arrays were fabricated at a set furnace temperature of 450 °C and collected at locations of 300 and 400 °C in the furnace. The morphology of the nanowire array samples was first investigated with SEM. From Figure 1a−c, well-aligned CdS and $Cd_{1-x}Zn_xS$ nanowire arrays, accompanied by a buffer layer about 1 μm thick laid on the silicon substrate surface, were observed. The nanowires were 30 nm in diameter and 500−900 nm in length. The corresponding XRD patterns of the as-grown CdS deposits collected at 300 °C and $Cd_{1-x}Zn_xS$ deposits collected at 300 and 400 °C and annealed at 500 °C for 48 h are shown in Figure 1d. Also included in Figure 1d are the XRD patterns of the reference hexagonal CdS crystals (JCPDS file no. 06−0314), ternary $Cd_{0.72}Zn_{0.28}S$ crystals (JCPDS file no. 40−0836), and $Cd_{0.22}Zn_{0.78}S$ crystals (JCPDS file no. 35−1469) for comparison purposes. For the CdS deposits, a predominant diffraction peak at 2θ of around 26.4° corresponding to the (0002) planes of the hexagonal crystalline structure of the reference CdS (at $2\theta = 26.45°$) was observed, indicating that the as-grown CdS deposits were hexagonal in the crystalline structure and possessed a structural orientation along its *c*-axis. For the annealed $Cd_{1-x}Zn_xS$ deposits collected at 300 °C, the predominant peak at 2θ of 26.9° lies between the (0002) peaks of the reference CdS (at $2\theta = 26.45°$) and ternary $Cd_{0.72}Zn_{0.28}S$ crystals (at $2\theta = 27.10°$), indicating that the *x* value of the $Cd_{1-x}Zn_xS$ nanowire arrays collected at 300 °C is less than 0.28 and greater than 0. As for the annealed $Cd_{1-x}Zn_xS$ deposits collected at 400 °C, the predominant peak at 2θ of 27.4° lies between the (0002) peaks of the reference ternary $Cd_{0.72}Zn_{0.28}S$ (at $2\theta = 27.10°$) and ternary $Cd_{0.22}Zn_{0.78}S$ (at $2\theta = 27.85°$), indicating that the *x* value of the $Cd_{1-x}Zn_xS$ nanowire arrays collected at 400 °C is greater than 0.28 but less than 0.78. The presence of the predominant diffraction peak of the (0002) plane reflects the fact that the nanowires were well-aligned vertical to the substrate and grew along the preferential growth direction of [0002]. The alignment, however, was not perfect so that minor diffractions still appear from other planes. Also note that the predominant diffraction peak shifts to larger 2θ values with increasing the Zn incorporation (greater *x*). This is expected since Zn is smaller than Cd in its atomic radius and because its replacement of Cd tends to reduce the corresponding lattice constant, thus resulting in larger 2θ values. Note further that higher collection temperatures provide more thermal energy necessary to overcome the activation energy associated with the replacement process of Cd with Zn and thus lead to more Zn incorporation for the alloy nanowire arrays collected at 400 °C than at 300 °C.

The detailed crystalline structures of the nanowires freed from the substrate were further examined with TEM and HRTEM. Figure 2a shows a TEM image of a single CdS nanowire with a diameter of about 30 nm. The dot pattern of the corresponding selected area electron diffraction (SAED) pattern suggests the single-crystalline nature of the CdS nanowires. The SAED pattern can be indexed to the reflections of hexagonal CdS crystals, consistent with the corresponding XRD pattern shown in Figure 1d. Figure 2b shows the HRTEM image taken on the edge of a single CdS nanowire. The lattice-resolved image reveals the lattice spacing of 0.67 nm, in good agreement with the *d*-spacing of the (0001) planes of hexagonal CdS. The axis of the CdS nanowires was found to be parallel to the [0001] direction, indicating that the CdS nanowires grew along the [0001] direction. This observation agrees with the XRD observation of the CdS nanowire arrays with the diffraction peak of (0002) being dominant over the other diffraction peaks (Figure 1d).

For the alloy nanowires, their shape, length, and diameter are similar to those of the CdS nanowires as can be seen from Figure 2c,e. TEM-EDS analyses showed a uniform elemental composition along the axial direction of the nanowires with atomic ratios of Cd/Zn of about 79:21 and 56:44 for the alloy nanowires collected at 300 and 400 °C, respectively. Dot patterns were observed in the corresponding SAED images for the two alloy samples, suggesting that these ternary nanowires were also single-crystalline. The SAED patterns can be indexed to the reflections of the hexagonal crystalline structure, consistent with the conclusion drawn from the corresponding XRD results. The lattice-resolved image taken on a single $Cd_{1-x}Zn_xS$ nanowire collected at 300 °C is shown in Figure 2d. The interlayer spacing of about 0.66 nm corresponds well to the *d*-spacing of the (0001) planes of the ternary $Cd_{1-x}Zn_xS$ hexagonal crystal as determined from the XRD analysis ($d(0002) = 0.331$ nm). As to the $Cd_{1-x}Zn_xS$ sample collected at 400 °C, a 0.64 nm interlayer spacing was observed, in good agreement with the *d*-spacing of the (0001) planes of hexagonal $Cd_{1-x}Zn_xS$, as determined from the XRD analysis ($d(0002) = 0.325$ nm). Note that the interlayer spacing of the (0001) planes decreases with increasing the Zn incorporation in the nanowire. This is expected from the consideration of the relative atomic size of Cd and Zn, as discussed in the section on XRD. The axes of both $Cd_{1-x}Zn_xS$ nanowire samples were parallel to the [0001] direction, indicating that these $Cd_{1-x}Zn_xS$ nanowires grew along the [0001] direction. This observation is in good agreement with the XRD analyses of the $Cd_{1-x}Zn_xS$ nanowire arrays with the (0002) diffraction peak being dominant over the other diffraction peaks (Figure 1d).

The PL spectra for the plain CdS and $Cd_{1-x}Zn_xS$ nanowire arrays are compared in Figure 3. For the CdS nanowires, a typical near band edge emission with the peak centering around 535 nm was observed ($E_g = 2.5$ eV,[15a,b] corresponging to an

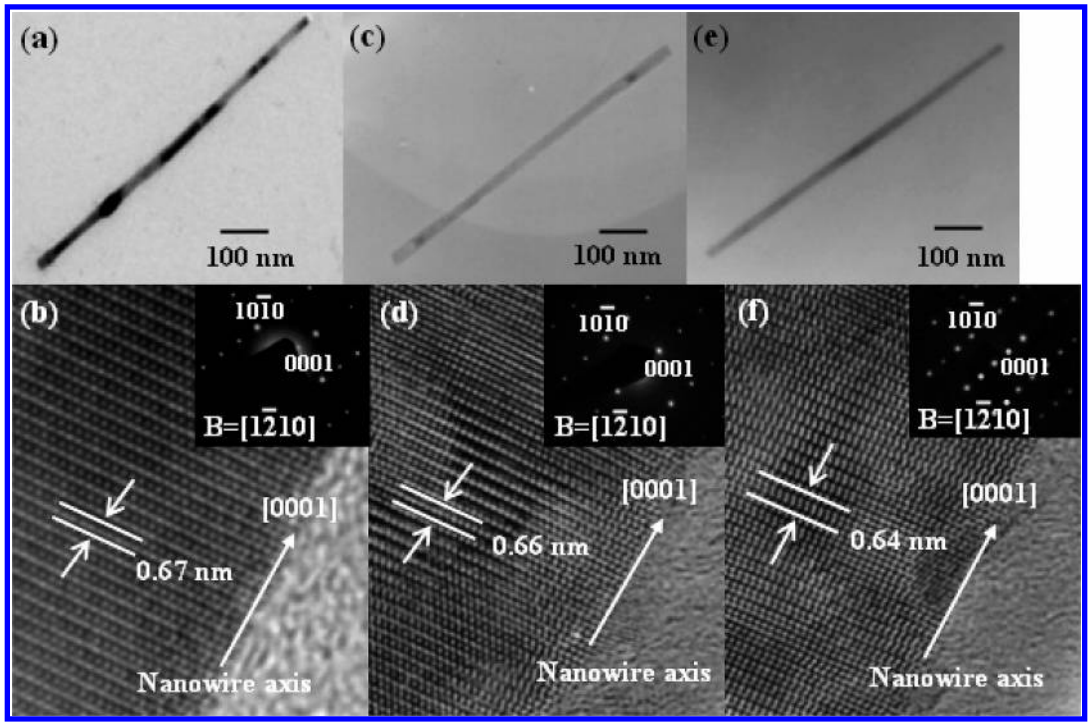

Figure 2. TEM images taken on a single (a) CdS nanowire, (c) $Cd_{1-x}Zn_xS$ nanowire collected at 300 °C, and (e) $Cd_{1-x}Zn_xS$ nanowire collected at 400 °C. Their corresponding HRTEM images are shown in panels b, d, and f, respectively.

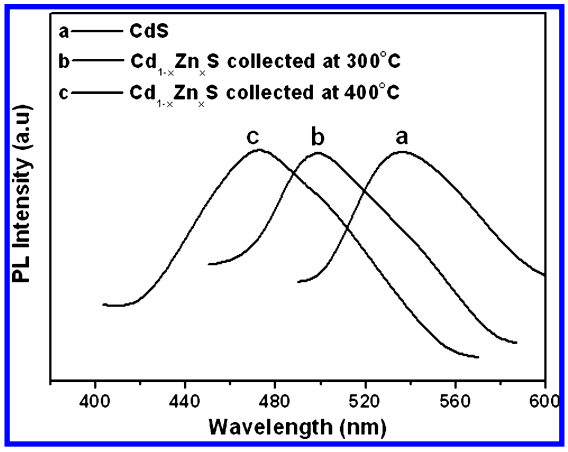

Figure 3. PL spectra of CdS deposits and $Cd_{1-x}Zn_xS$ deposits collected at 300 and 400 °C.

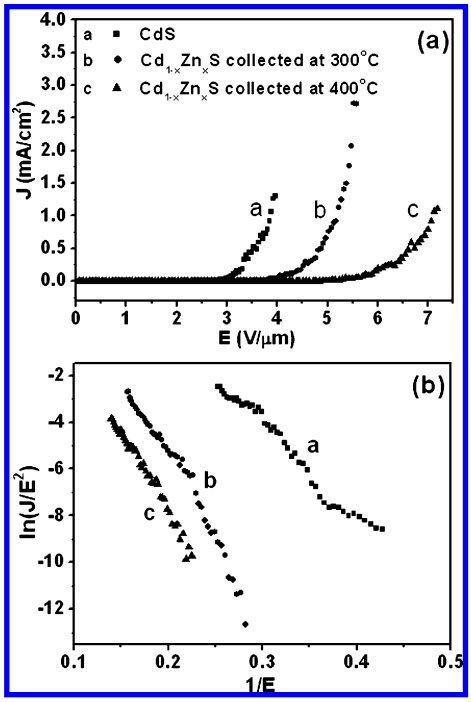

Figure 4. (a) $J-E$ curves and (b) corresponding F−N plots for CdS deposits and $Cd_{1-x}Zn_xS$ deposits collected at 300 and 400 °C. Interelectrode spacing was set at 200 μm.

absorption edge of 496 nm). This emission originated from the radiative band-to-band recombination process of excitons. As to the ternary $Cd_{1-x}Zn_xS$ nanowires collected at 300 and 400 °C, emission bands at around 498 and 473 nm were observed, respectively. To identify the essence of these emission bands from the ternary $Cd_{1-x}Zn_xS$ nanowires, we presented the following argument. The bulk band gap energy for ternary $Cd_{1-x}Zn_xS$ alloys can be described with the following equation:[6a]

$$E_g(x) = 2.5 + 0.59x + 0.61x^2 \text{ (eV)} \quad (1)$$

The atomic ratios of Zn/(Zn + Cd) for the $Cd_{1-x}Zn_xS$ nanowires collected at 300 and 400 °C were estimated to be 0.21 and 0.44, respectively, from the corresponding TEM-EDS analyses. By substituting the estimated atomic ratios of 0.21 and 0.44 into eq 1, one can obtain a theoretical energy band gap of 2.65 eV (a corresponding absorption edge of 467 nm) for the nanowires collected at 300 °C and 2.88 eV (a corresponding absorption edge of 431 nm) for the nanowires collected at 400 °C. In view of the closeness of the two PL emission bands with the corresponding theoretical absorption edges, the emission bands at around 498 and 473 nm may be attributed to the excitonic band-to-band radiative emission (near band edge emission) of the ternary $Cd_{1-x}Zn_xS$ nanowires. Note that the PL spectra of the three nanowire samples clearly demonstrate the emission tunability achieved with the adjustment in composition of the ternary nanowires. The incorporation of Zn to CdS enlarges the energy band gap and thus results in the blue-shifted emission bands of the products.

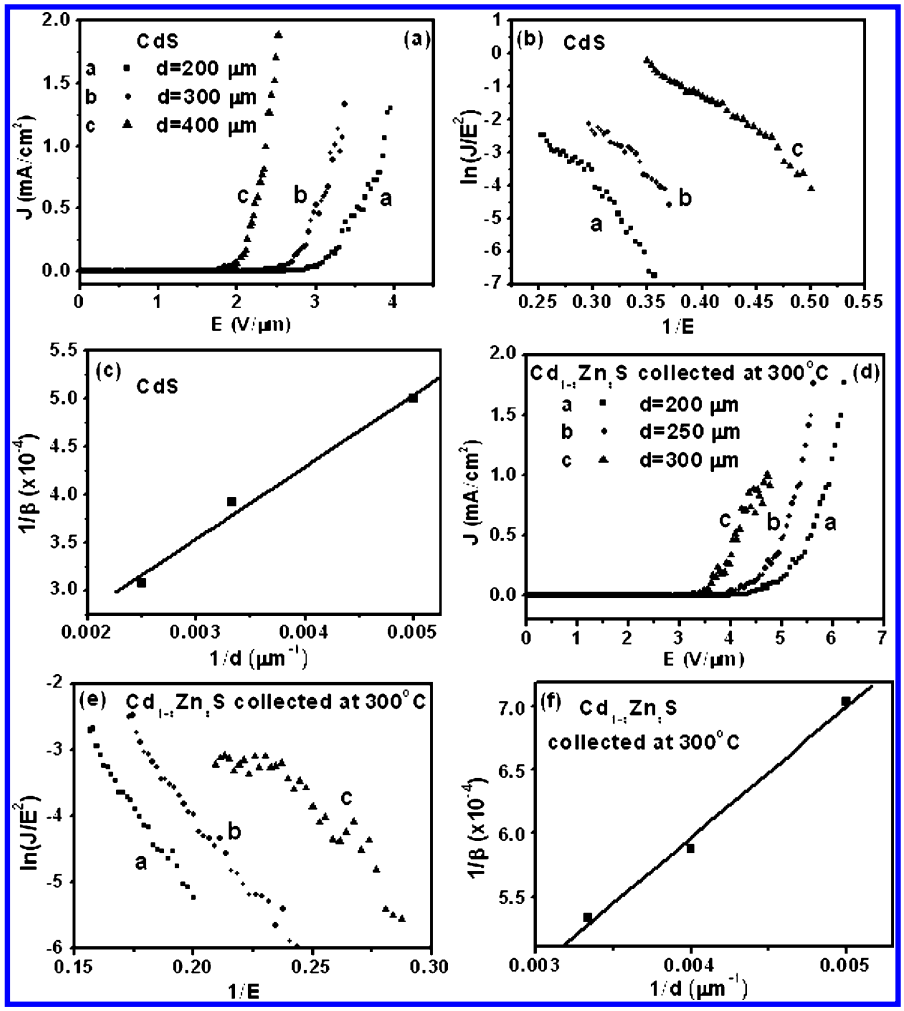

Figure 5. (a) $J-E$ curves, (b) corresponding F−N plot, and (c) corresponding plot of $1/\beta$ vs $1/d$ for CdS nanowire arrays at three different interelectrode spacings. Symbols used in the F−N plot refer to those used in panel a. (d) $J-E$ curves, (e) corresponding F−N plot, and (f) corresponding plot of $1/\beta$ vs $1/d$ for $Cd_{1-x}Zn_xS$ nanowire arrays collected at 300 °C at three different interelectrode spacings. Symbols used in panel e refer to those in panel d.

The field emission properties of the plain CdS and ternary $Cd_{1-x}Zn_xS$ nanowire arrays were next investigated. They were measured under the setting of an interelectrode spacing of 200 μm and a pressure of 10^{-6} Torr for the vacuum chamber. Figure 4a shows the plot of the field emission current density (J) versus the applied electric field (E) for the three different samples. The turn-on fields, defined as the field required to achieve a current density of 0.1 μA/cm^2, were estimated to be 2.2, 3.6, and 4.1 V/μm for the CdS nanowire arrays, $Cd_{1-x}Zn_xS$ nanowire arrays collected at 300 °C, and $Cd_{1-x}Zn_xS$ nanowire arrays collected at 400 °C, respectively. The field emission characteristics were further analyzed with the F−N theory. According to the F−N law, the relationship between J and E can be described as follows:[16]

$$J = (A\beta^2E^2/\Phi)\exp(-B\Phi^{3/2}/\beta E) \qquad (2)$$

Here, Φ is the work function of the emitter, β is the field enhancement factor, and A and B are constants with values of 1.56×10^{-10} (A V^{-2} eV) and 6.83×10^{-10} (V eV$^{-3/2}$ m^{-1}), respectively. Figure 4b shows the corresponding F−N plot for the CdS and $Cd_{1-x}Zn_xS$ nanowire arrays. The linearity of the data points observed at high electric fields indicates that the field emission in the present nanowires is a quantum mechanical tunneling process and obeys the F−N law.[17] From the slopes of the fitted straight lines in the F−N plot and by assuming work functions of 5.01, 5.09, and 5.18 eV for CdS, $Cd_{1-x}Zn_xS$ collected at 300 °C, and $Cd_{1-x}Zn_xS$ collected at 400 °C, respectively,[18] the field enhancement factors were estimated to be about 2000, 1421, and 1180 for CdS and the two $Cd_{1-x}Zn_xS$ nanowire arrays collected at 300 and 400 °C, respectively. It is generally accepted that β is related to the geometry, structure, and density of the nanostructures examined.[19] In this work, the three samples all possessed similar structural characteristics, morphology, length, and diameter. Hence, the differences in β among them mainly came from compositional diversity in the nanowires. In other words, the incorporation of Zn into CdS led to a depression in the β value. The incorporation of Zn into CdS caused an increase in the energy gap, resulting in a decrease in the free carrier concentration and an increase in resistivity.[20] The increased resistivity would hinder the free electrons from moving through the nanowires and thus significantly raise the voltage drop along the nanowires when electrons with the same current density were transported.[21] As a result, a depression in field emission efficiency was observed for the $Cd_{1-x}Zn_xS$ nanowire arrays as compared to the plain CdS nanowires. Moreover, the further incorporated amount of Zn led to an even worse field emission ability for the $Cd_{1-x}Zn_xS$ nanowire arrays collected at 400 °C.

To obtain a more intrinsic characterization of the field emission efficiency of the three nanowire arrays, we investigated the relationship between β and d by adopting the two-region

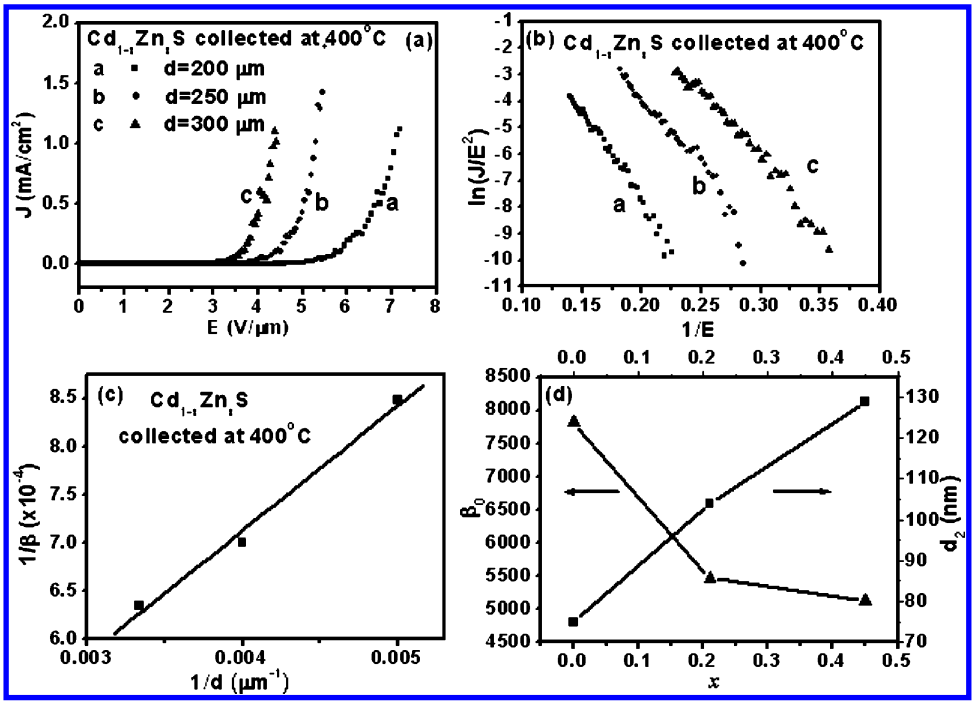

Figure 6. (a) $J-E$ curves, (b) corresponding F−N plot, and (c) corresponding plot of $1/\beta$ vs $1/d$ for $Cd_{1-x}Zn_xS$ nanowire arrays collected at 400 °C at three different interelectrode spacings. (d) β_0 and d_2 as a function of composition (x) for $Cd_{1-x}Zn_xS$ nanowire arrays. Symbols used in the corresponding F−N plot refer to those used in panel a.

field emission model proposed by Zhong et al. [14a] The model gives the following relation for β and d:

$$1/\beta = d_2/d + 1/\beta_0 \quad (3)$$

Here, d_2 is the thickness of the field enhanced region and β_0 is the absolute field enhancement factor. The parameter β_0 is independent of d and V and serves as a more intrinsic measure of the field emission efficiency. Evidently, one can obtain d_2 and β_0 values from the slope and intercept of the plot of $1/\beta$ versus $1/d$. Figure 5a shows the $J-E$ plot for the CdS nanowire arrays at different d values. The turn-on fields (the required field for $J = 0.1$ μA/cm^2) were estimated to be 2.2, 1.9, and 1.4 V/μm at $d = 200$, 300, and 400 μm, respectively. From the corresponding F−N plot shown in Figure 5b, β values were estimated to be about 2000, 2551, and 3225 at $d = 200$, 300, and 400 μm, respectively. Figure 5c depicts the relationship between $1/\beta$ and $1/d$. From the slope and intercept of the fitted straight line shown in Figure 5c, d_2 and β_0 of the TRFE model were determined to be around 75 nm and 7813, respectively. The same procedure was applied to the two ternary $Cd_{1-x}Zn_xS$ nanowire arrays for the determination of d_2 and β_0. For the $Cd_{1-x}Zn_xS$ nanowire arrays collected at 300 °C, d_2 and β_0 were calculated to be about 104 nm and 5465, respectively. As to the $Cd_{1-x}Zn_xS$ nanowire arrays collected at 400 °C, values of d_2 of 129 nm and β_0 of 5128 were obtained. The values of β_0 determined for the present three nanowire arrays are comparable to that of the carbon nanotubes grown on silicon wafers ($\beta_0 =$ 7900)[14a] and much larger than that of the Al-doped ZnO emitter ($\beta_0 = 1845$).[14b] With this, the present nanowire arrays should be considered as a promising alternative for field emission applications. It is worth mentioning that the thick buffer layers did not hinder much the field emission performance of the nanowire arrays. This is probably due to the excellent alignment and continuity in the crystallographic structure of the buffer layer with the nanowires as discussed in our preliminary report for the plain CdS case.[10] In that study, the growth directions in the buffer layer, buffer−wire interface, and nanowires were found all to be [0001], without lattice mismatch and defects existing at the buffer−wire interface.

Figure 6d shows how composition, quantified as x, affects the value of β_0 and d_2. For the present case, the incorporation of Zn to CdS (increasing x) suppresses the field emission of the nanowires (decreasing β_0). Interestingly, the trends for β_0 and d_2 are opposite of each other. When the field emission ability of the emitter improves (increasing β_0), the emitter needs only a thinner active thickness to achieve the same level of emission (decreasing d_2). This opposite trend in β_0 and d_2 also occurred in carbon nanotubes grown on silicon wafers (7900 and 540 nm) and iron tips (25000 and 160 nm).[14a]

A possible growth mechanism for the formation of the CdS and $Cd_{1-x}Zn_xS$ nanowire arrays is proposed as follows. Note that no catalysts were used and that no guiding heads were found at the tips of the as-grown nanowires. As a result, the commonly encountered anisotropic growth mechanism of VLS cannot account for the growth of the 1-D nanostructures obtained in this work. For typical hexagonal crystals, such as ZnS, ZnO, and CdS, growth of the nanocrystals with a preferential direction along their c-axes, the direction possessing the fastest growth rate, without the presence of guiding catalysts or templates was commonly observed in the literature.[8a,10,22] In the present work, with suitable control of the deposition conditions, growth of CdS and $Cd_{1-x}Zn_xS$ nanocrystals along their c-axis directions to form the nanowire arrays was also achieved. Here, we took the nanowire arrays of $Cd_{1-x}Zn_xS$ collected at 400 °C as an example to further interpret the growth steps during the deposition process. As shown in the SEM image of Figure 7a, co-feeding of Cd33 and Zn22, the precursors for CdS and ZnS, respectively, led to the formation of the $Cd_{1-x}Zn_xS$ particle films at the early stage of the deposition (1 h). The corresponding XRD patterns, as shown in Figure 8, provided some more insight on the growth process. For the $Cd_{1-x}Zn_xS$ deposits collected at 400 °C after a 20 min deposition, a predominant diffraction peak at 2θ of around 27.8° was observed. This diffraction peak, corresponding to the (0002) plane of the hexagonal crystalline

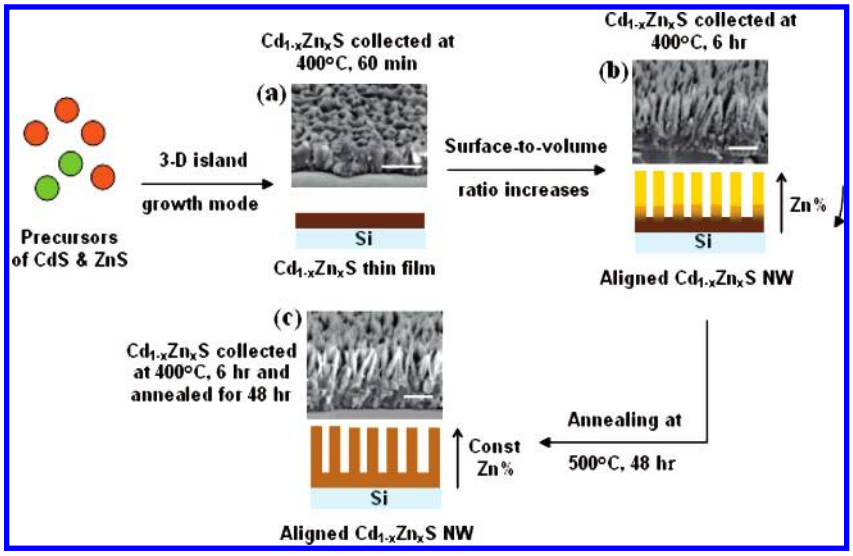

Figure 7. Plausible growth mechanism for the formation of $Cd_{1-x}Zn_xS$ nanowire arrays. Scale bar is 1 μm.

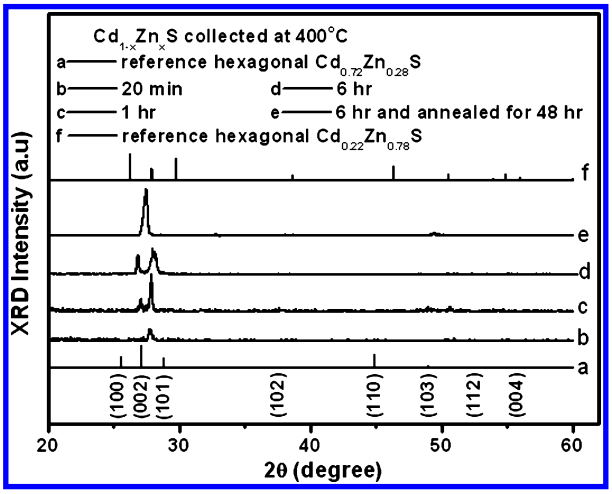

Figure 8. XRD patterns of $Cd_{1-x}Zn_xS$ deposits collected at 400 °C at different deposition times.

phase, lay between the (0002) peaks of the reference $Cd_{0.72}Zn_{0.28}S$ (at $2\theta = 27.10°$) and $Cd_{0.22}Zn_{0.78}S$ crystals (at $2\theta = 27.85°$), implying that the as-grown thin films were composed of $Cd_{1-x}Zn_xS$ with $0.28 < x < 0.78$. As for the sample obtained with a deposition time of 60 min, two diffraction peaks appeared. These two peaks were both assigned to the reflection of the (0002) planes of the hexagonal phase. One of them lay between the positions of the (0002) peaks of the hexagonal CdS (at $2\theta = 26.45°$) and ternary $Cd_{0.72}Zn_{0.28}S$ (at $2\theta = 27.10°$) crystals. The other was, however, located between the positions of the (0002) peaks of the hexagonal $Cd_{0.72}Zn_{0.28}S$ (at $2\theta = 27.10°$) and $Cd_{0.22}Zn_{0.78}S$ (at $2\theta = 27.85°$) crystals. The previous observation of the two distinct diffraction peaks contributed by the (0002) planes implies that a significant compositional variation existed in the deposit. The early grown portion was richer in Zn than the later grown portion. The appearance of the particle film in the initial stage was attributed to the 3-D island growth mode, due to the large difference in surface free energy and significant lattice mismatch between the growing $Cd_{1-x}Zn_xS$ and the silicon substrate.[23]

Gibbs derived a general formula (eq 4) to describe the equilibrium crystal growth process at constant temperature (T) and volume (V) as was used in ref 24. This derivation was based on the minimization of the Helmholtz free energy during the phase transition. The relation was given as

$$P_c - P_v = \Sigma\delta(\sigma_i S_i)/\delta V_c \quad (4)$$

Here, P_c is the pressure of the crystal phase, P_v is the pressure of the vapor phase, σ_i and S_i are the surface energy and surface area of species i, respectively, and V_c is the volume of the crystal phase. At the late stage of deposition, the depletion in the fed precursor led to a decrease in the precursor vapor pressure. From the previous equation, the decrease in the precursor vapor pressure (P_v) resulted in an increase in the surface-to-volume ratio ($\delta S_i/\delta V_c$). This increased surface-to-volume ratio at the late stage of the deposition turned to drive the crystal growth

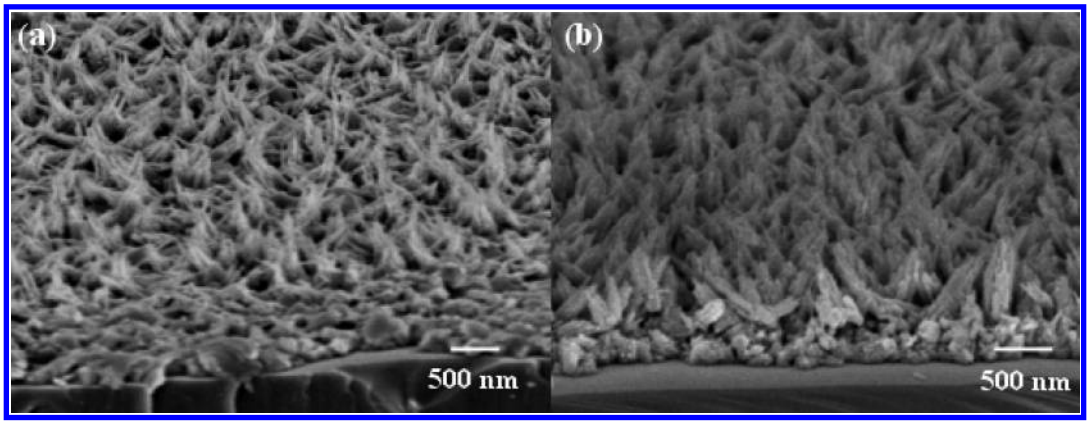

Figure 9. SEM images of CdS nanowire arrays collected 300 °C using a precursor, Cd33, of (a) 0.01 g and (b) 0.02 g.

to proceed in an anisotropic growth mode to favor a larger surface-to-volume ratio inherent in the nanowire structure. Therefore, the growth of anisotropic nanostructures dominated the deposition after an initial period of 3-D island growth, resulting in nanowires grown on top of the first-formed particle films (a 1 μm thick buffer layer), as shown in the SEM image in Figure 7b. Before the annealing process, the buffer layer was richer in Zn than the nanowire zone, as evidenced from the two distinct diffraction peak patterns (*d*) in Figure 8. After the annealing treatment at 500 °C for 48 h, the whole deposit homogenized to one single composition as can be inferred from the single diffraction peak at 2θ of 27.4° of spectrum e in Figure 8. This single diffraction peak lay between the two diffraction peaks before annealing, indicating that the composition was averaged from the two compositions of the buffer layer and nanowire zones before annealing. The morphology of the nanowire array lying on top of the buffer layer remained unchanged after the annealing treatment. Note that annealing is commonly utilized in materials syntheses to achieve uniformity in both composition and crystallinity desired for final product applications.[25]

According to the growth mechanism proposed previously, the consumption of the precursors and the depletion of the precursor vapors triggered the formation of 1-D nanowires. One may argue that if the amount of the precursors fed was limited to some low levels at the beginning, would the anisotropic growth mode be dominant throughout the whole deposition process without the formation of the buffer layer? To clarify this issue, depositions using limited amounts of precursors, 0.01 and 0.02 g of Cd33 as compared to 0.1 g for the normal case, were run. Figure 9 shows the surface morphology of the resulting CdS deposits on a silicon substrate. Nanowires were again found to grow on top of a buffer layer, only the thickness of the buffer layer was now decreased to 300 nm as compared to the 1 μm thick buffer layer for the normal case. Evidently, the thickness of the buffer layer decreased because of the decrease in precursor quantity available for deposition. Interestingly, the formation of the buffer layer before the anisotropic growth can occur is inevitable in the present process due to the congenital lattice mismatch and the significant difference in surface free energy between the substrate and the growing materials.

Conclusion

Plain CdS and ternary $Cd_{1-x}Zn_xS$ nanowire arrays were successfully fabricated via a noncatalytic and template-free MOCVD process. These nanowires were grown accompanied with a 1 μm thick buffer layer lying on the substrate surface. The nanowires were 20−40 nm in diameter and 500−900 nm in length. The XRD, HRTEM, and SAED analyses confirmed the single-crystalline structures and ternary alloy compositions of the synthesized nanowires. The nanowires of CdS and $Cd_{1-x}Zn_xS$ all possessed a preferential growth direction along their *c*-axes, the [0001] direction. The *x* values of the $Cd_{1-x}Zn_xS$ nanowires were determined by TEM-EDS to be 0.21 and 0.44 for samples collected at 300 and 400 °C, respectively. Their PL characterization demonstrated the color tunability achieved with composition adjustment in the ternary nanowires. As to the field emission characteristics, the CdS nanowires possessed better field emission properties, lower turn-on fields, and a larger absolute field enhancement factor, as compared to the ternary $Cd_{1-x}Zn_xS$ nanowires. The incorporation of Zn into CdS significantly increased the resistivity of the nanowire arrays, resulting in an increase in the voltage drop along the nanowires, which in turn suppressed the field emission efficiency. An important parameter, the absolute field enhancement factor (β_0), to more intrinsically characterize the field emission performance of an emitter was estimated for the plain CdS and ternary $Cd_{1-x}Zn_xS$ nanowire arrays for the first time. The high values of β_0 observed in the present CdS based nanowire arrays make them a promising candidate material for field emission applications.

Acknowledgment. The authors acknowledge financial support from the National Science Council of the Republic of China (Taiwan) under Grant NSC-95-2221-E-007-194.

References and Notes

(1) (a) Hsu, Y.-J.; Lu, S.-Y.; Lin, Y.-F. *Adv. Funct. Mater.* **2005**, *15*, 1350. (b) Hsu, Y.-J.; Lu, S.-Y. *Chem. Commun.* **2004**, 2102. (c) Lin, Y.-F.; Hsu, Y.-J.; Lu, S.-Y.; Chiang, W.-S. *Nanotechnology* **2006**, *17*, 4773. (d) Chueh, Y.-L.; Hsieh, C.-H.; Chang, M.-T.; Chou, L.-J.; Lao, C.-S.; Song, J. H.; Gan, J.-Y.; Wang, Z.-L. *Adv. Mater.* **2007**, *19*, 143.

(2) (a) Wu, Y.; Fan, R.; Yang, P. *Nano Lett.* **2002**, *2*, 83. (b) Gudiksen, M. S.; Lauhon, L. J.; Wang, J.; Smith, D. C.; Lieber, C. M. *Nature* **2002**, *415*, 617.

(3) (a) Pan, A.; Yang, H.; Liu, R.; Yu, R.; Zou, B.; Wang, Z. L. *J. Am. Chem. Soc.* **2005**, *127*, 15692. (b) Liu, Y.; Zapien, J. A.; Shan, Y. Y.; Geng, C. Y.; Lee, C. S.; Lee, S. T. *Adv. Mater.* **2005**, *17*, 1372. (c) Venugopal, R.; Lin, P.-I.; Chen, Y.-T. *J. Phys. Chem. B* **2006**, *110*, 11691.

(4) Xia, Y.; Yang, P.; Sun, Y.; Wu, Y.; Mayers, B.; Gates, B.; Yin, Y.; Kim, F.; Yan, H. *Adv. Mater.* **2003**, *15*, 353.

(5) (a) Wang, A.; Dai, J.; Cheng, J.; Chudzik, M. P.; Marks, T. J.; Chang, R. P. H.; Kannewurf, C. R. *Appl. Phys. Lett.* **1998**, *73*, 327. (b) Young, D. L.; Williamson, D. L.; Coutts, T. J. *J. Appl. Phys.* **2002**, *91*, 1464.

(6) (a) Suslina, L. G.; Danasyuk, E. I.; Konnikov, S. G.; Federov, D. L. *Sov. Phys. Semicond.* **1976**, *10*, 1093. (b) Korgel, B. A.; Monbouquette, H. G. *Langmuir* **2000**, *16*, 3588. (c) Zhong, X.; Han, M.; Dong, Z.; White, T. J.; Knoll, W. *J. Am. Chem. Soc.* **2003**, *125*, 8589. (d) Liang, Y.; Zhai, L.; Zhao, X.; Xu, D. *J. Phys. Chem. B* **2005**, *109*, 7120.

(7) Rincon, M. E.; Martinez, M. W.; Miranda-Hernandez, M. *Sol. Energy Mater. Sol. Cells* **2003**, *77*, 25.

(8) (a) Moore, D. F.; Ding, Y.; Wang, Z. L. *J. Am. Chem. Soc.* **2004**, *126* 14372. (b) Hu, C.-C.; Chang, K.-H.; Lin, M.-C.; Wu, Y.-T. *Nano Lett.* **2006**, *6*, 2690.

(9) (a) Wang, Z. L.; Song, J. *Science* **2006**, *312*, 242. (b) Law, M.; Greene, L. E.; Johoson, J. C.; Saykally, R.; Yang, P. *Nat. Mater.* **2005**, *4*, 455.

(10) Lin, Y.-F.; Hsu, Y.-J.; Lu, S. Y.; Kung, S.-C. *Chem. Commun.* **2006**, 2391.

(11) (a) Wu, J. J.; Liu, S. C. *J. Phys. Chem. B* **2002**, *106*, 9546. (b) Park, W. I.; Kim, D. H.; Jung, S. W.; Yi, G. C. *Appl. Phys. Lett.* **2002**, *80*, 4232.

(12) Zhao, Q.; Zhang, H. Z.; Zhu, Y. W.; Feng, S. Q.; Sun, X. C.; Xu, J.; Yu, D. P. *Appl. Phys. Lett.* **2005**, *86*, 203115.

(13) Lee, C. Y.; Tseng, T. Y.; Li, S. Y.; Lin, P. *Nanotechnology* **2005**, *16*, 1105.

(14) (a) Zhong, D. Y.; Zhang, G. Y.; Liu, S.; Sakurai, T.; Wang, T.; Wang, E. G. *Appl. Phys. Lett.* **2002**, *80*, 506. (b) Xue, X. Y.; Li, L. M.; Yu, H. C.; Chen, Y. J.; Wang, Y. G.; Wang, T. H. *Appl. Phys. Lett.* **2006**, *89*, 43118. (c) Xiang, B.; Wang, Q. X.; Wang, Z.; Zhang, X. Z.; Liu, L. Q.; Xu, J.; Yu, D. P. *Appl. Phys. Lett.* **2005**, *86*, 243103. (d) Chen, Y. J.; Li, Q. H.; Liang, Y. X.; Wang, T. H.; Zhao, Q.; Yu, D. P. *Appl. Phys. Lett.* **2004**, *85*, 5682.

(15) (a) Hsu, Y.-J.; Lu, S.-Y. *Appl. Phys. A* **2005**, *81*, 573. (b) Hsu, Y.-J.; Lu, S.-Y. *Langmuir* **2004**, *20*, 23. (c) O'Brien, P.; Walsh, J. R.; Watson, I. M.; Motevalli, M.; Henriksen, L. *J. Chem. Soc., Dalton Trans.* **1996**, 2491.

(16) Fowler, R. H.; Nordheim, L. W. *Proc. R. Soc. London, Ser. A* **1928**, *119*, 173.

(17) Tang, C.; Bando, Y. *Appl. Phys. Lett.* **2003**, *83*, 659.

(18) Swank, R. K. *Phys. Rev.* **1967**, *153*, 844. The work functions of CdS and ZnS were determined to be 5.01 and 5.4 eV, respectively, in the reference. We estimated the work functions of $Cd_{1-x}Zn_xS$ nanowires collected at 300 and 400 °C to be 5.09 and 5.18 eV, respectively, with linear interpolation.

(19) (a) Lee, C. J.; Lee, T. J.; Lyu, S. C.; Zhang, Y.; Ruh, H.; Lee, H. J. *Appl. Phys. Lett.* **2002**, *81*, 3648. (b) Liu, J.; Huang, X.; Li, Y.; Ji, X.; Li, Z.; He, X.; Sun, F. *J. Phys. Chem. C* **2007**, *111*, 4990. (c) Wang, X.; Zhou, J.; Lao, C.; Song, J.; Xu, N.; Wang, Z. L. *Adv. Mater.* **2007**, *19*, 1627.

(20) Gaewdang, N.; Gaewdang, T. *Mater. Lett.* **2005**, *59*, 3577.

(21) Xu, C. X.; Sun, X. W.; Chen, B. J. *Appl. Phys. Lett.* **2004**, *84*, 1540.

(22) (a) Peterson, R. B.; Fields, C. L.; Gregg, B. A. *Langmuir* **2004**, *20*, 5114. (b) Wang, Z.; Qian, X. F.; Yin, J.; Zhu, Z. K. *Langmuir* **2004**, *20*, 3441. (c) Liu, B.; Zeng, H. C. *Langmuir* **2004**, *20*, 4196. (d) Zhu, Y. C.; Bando, Y.; Xue, D. F.; Golberg, D. *Adv. Mater.* **2004**, *16*, 831.

(23) There is a large lattice mismatch between cubic Si(100) substrate and hexagonal $Cd_{1-x}Zn_xS$.

(24) (a) Zhang, B. P.; Binh, N. T.; Wakatsuki, K.; Segawa, Y.; Yamada, Y.; Usami, N.; Kawasaki, M.; Koinuma, H. *J. Phys. Chem. B* **2004**, *108*, 10899. (b) Markov, I. V. *Crystal Growth for Beginners, Fundamentals of Nucleation, Crystal Growth, and Epitaxy*; World Scientific: Singapore, 1996; p 13.

(25) (a) He, J. H.; Lao, C. S.; Chen, L. J.; Davidovic, D.; Wang, Z. L. *J. Am. Chem. Soc.* **2006**, *127*, 16376. (b) Chang, K.-W.; Wu, J.-J. *Adv. Mater.* **2005**, *17*, 241.